Electronic Supplementary Information

For

Syntheses, crystal structures and magnetic properties of a series of μ-phenoxo-$\mu_{1,1}$-carboxylato-$\mu_{1,3}$-carboxylato trinickel(II) compounds

Sagarika Bhattacharya, Sujit Sasmal, Luca Carrella, Eva Rentschler* and Sasankasekhar Mohanta*

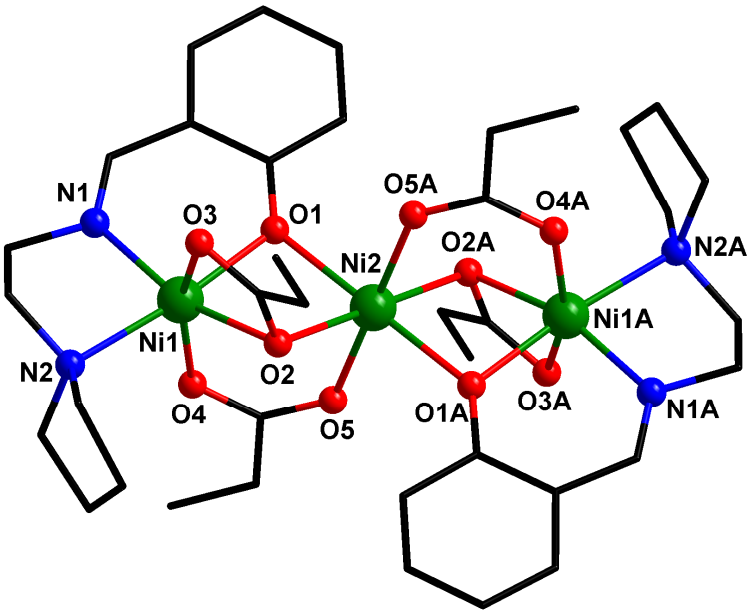

Fig. S1 Crystal structure of $[Ni^{II}_3(L^{sal-pyr})_2(Propionate)_4]$ (**1**). All the hydrogen atoms are omitted for clarity. Symmetry code: A, $1 - x, - y, - z$.

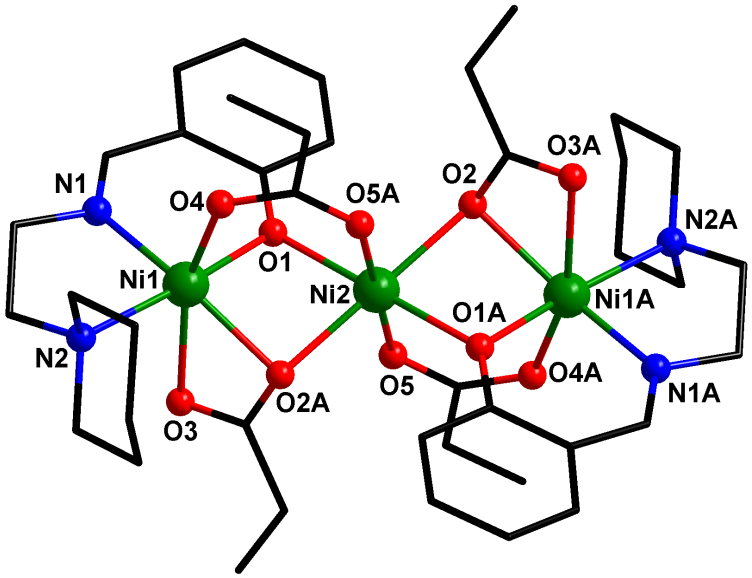

Fig. S2 Crystal structure of $[Ni^{II}_3(L^{sal-pip})_2(Propionate)_4]$ (**4**). All the hydrogen atoms are omitted for clarity. Symmetry code: A, $1 - x, 2 - y, 2 - z$.

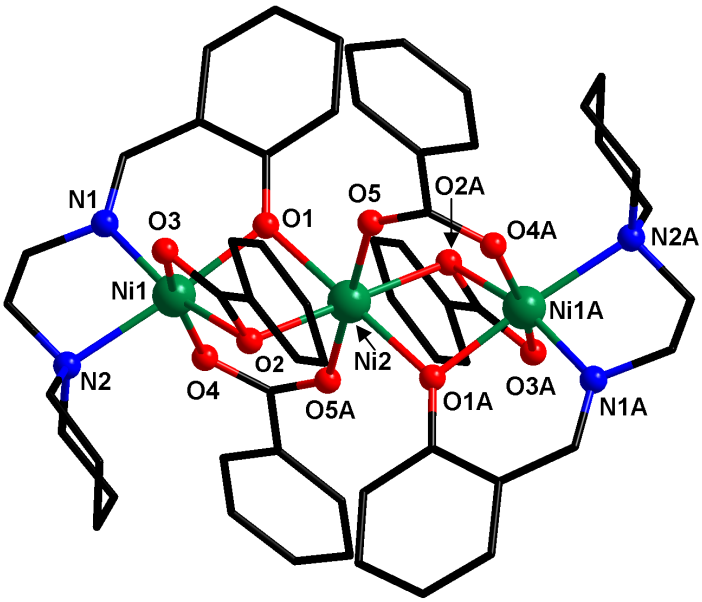

Fig. S3 Crystal structure of $[Ni^{II}_3(L^{sal-pip})_2(Benzoate)_4]\cdot CH_2Cl_2$ (**5**). All the hydrogen atoms and a dichloromethane molecule (solvent of crystallization) are omitted for clarity. Symmetry code: A, 0.5 – *x*, 0.5 – *y*, 1 – *z*.

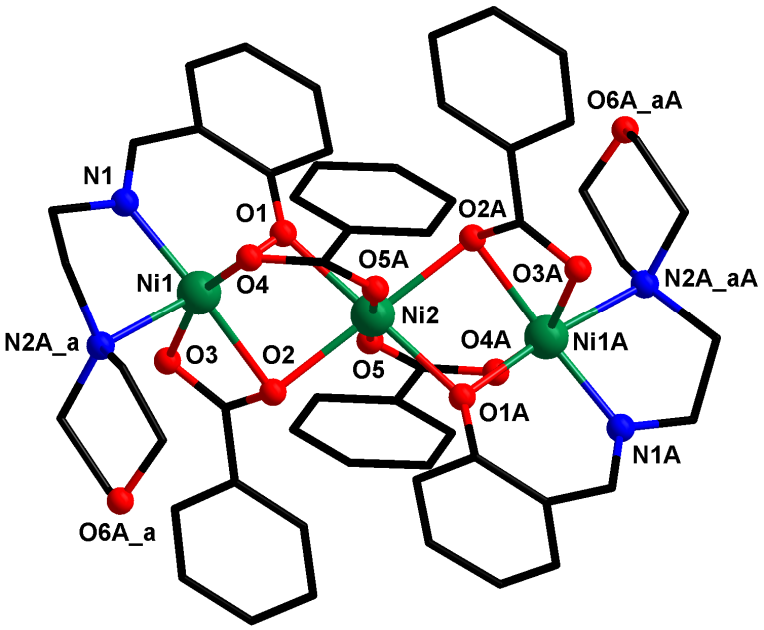

Fig. S4 Crystal structure of $[Ni^{II}_3(L^{sal-mor})_2(Benzoate)_4]\cdot 3CH_2Cl_2$ (**7**). Three dichloromethane molecule (solvents of crystallization) and all the hydrogen atoms are omitted for clarity. Symmetry code: A, 1 – *x*, 2 – *y*, 1 – *z*.

Table S1 Selected bond lengths (Å) and bond angles (°) in the coordination environments of the metal centers in Compound **2**. Symmetry codes A (for Unit-I): 1 – *x*, 1 – *y*, –*z*; B (for Unit-II): –*x*, 1 – *y*, 1 – *z*

2 (Unit-I)		**2** (Unit-II)	
Ni1–O1	2.007(6)	Ni3–O6	2.005(5)
Ni1–O2	2.148(6)	Ni3–O7	2.146(5)
Ni1–N1	1.992(8)	Ni3–N3	1.998(8)
Ni1–N2	2.157(9)	Ni3–N4	2.184(8)
Ni1–O3	2.183(6)	Ni3–O8	2.182(6)
Ni1–O4	2.020(6)	Ni3–O9	2.024(5)
Ni2–O1	2.114(6)	Ni4–O6	2.071(5)
Ni2–O1A	2.114(6)	Ni4–O6B	2.071(5)
Ni2–O2	2.125(6)	Ni4–O7	2.136(5)
Ni2–O2A	2.125(6)	Ni4–O7B	2.136(5)
Ni2–O5	1.997(6)	Ni4–O10	1.983(5)
Ni2–O5A	1.997(6)	Ni4–O10B	1.983(5)
Ni1···Ni2	3.051	Ni3···Ni4	3.066
N1–Ni1–O2	164.3(3)	N3–Ni3–O7	157.2(3)
N2–Ni1–O1	171.6(3)	N4–Ni3–O6	175.2(3)
O3–Ni1–O4	157.0(2)	O8–Ni3–O9	159.4(2)
N1–Ni1–N2	82.8(4)	N3–Ni3–N4	83.9(4)
N1–Ni1–O1	88.9(3)	N3–Ni3–O6	91.5(3)
N1–Ni1–O3	105.7(3)	N3–Ni3–O8	98.1(3)
N1–Ni1–O4	97.0(3)	N3–Ni3–O9	102.4(3)
N2–Ni1–O2	104.8(3)	N4–Ni3–O7	103.8(3)
N2–Ni1–O3	91.1(3)	N4–Ni3–O8	90.9(3)
N2–Ni1–O4	88.3(3)	N4–Ni3–O9	89.3(3)
O1–Ni1–O2	83.4(2)	O6–Ni3–O7	81.0(2)
O1–Ni1–O3	91.4(2)	O6–Ni3–O8	91.0(2)
O1–Ni1–O4	92.5(2)	O6–Ni3–O9	90.5(2)
O2–Ni1–O3	61.0(2)	O7–Ni3–O8	60.8(2)
O2–Ni1–O4	97.0(2)	O7–Ni3–O9	99.2(2)
O1–Ni2–O1A	179.999(1)	O6–Ni4–O6B	179.999(1)
O2–Ni2–O2A	179.998(1)	O7–Ni4–O7B	180.0
O5–Ni2–O5A	179.998(1)	O10–Ni4–O10B	179.999(1)
O1–Ni2–O2	81.5(2)	O6–Ni4–O7	79.8(2)
O1–Ni2–O2A	98.5(2)	O6–Ni4–O7B	100.2(2)
O1–Ni2–O5	90.1(2)	O6–Ni4–O10	92.3(2)
O1–Ni2–O5A	89.9(2)	O6–Ni4–O10B	87.7(2)
O2–Ni2–O5	89.9(2)	O7–Ni4–O10	89.4(2)
O2–Ni2–O5A	90.1(2)	O7B–Ni4–O10	90.6(2)
Ni1–O1–Ni2	95.5(3)	Ni3–O6–Ni4	97.6(2)
Ni1–O2–Ni2	91.1(2)	Ni3–O7–Ni4	91.45
Ni1···Ni2···Ni1A	180.00	Ni3···Ni4···Ni3B	180.00

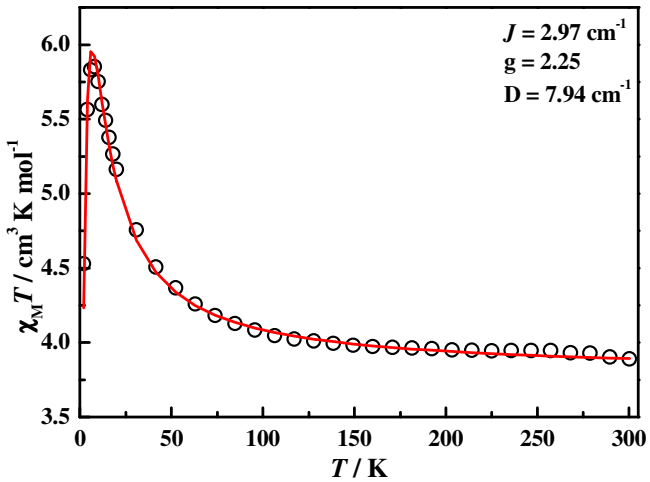

Fig. S5 Fittings of the $\chi_M T$ vs T of $[Ni^{II}_3(L^{sal-pyr})_2(Benzoate)_4]\cdot CH_3CN$ (**2**) between 2.0 and 300.0 K. The experimental data is shown as black circles and the red line corresponds to the theoretical values.

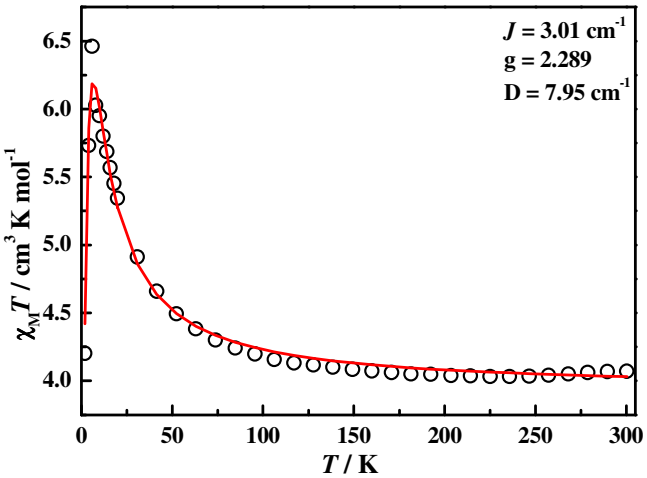

Fig. S6 Fittings of the $\chi_M T$ vs T of $[Ni^{II}_3(L^{sal-pip})_2(Acetate)_4]\cdot 2CH_3CN$ (**3**) between 2.0 and 300.0 K. The experimental data is shown as black circles and the red line corresponds to the theoretical values.

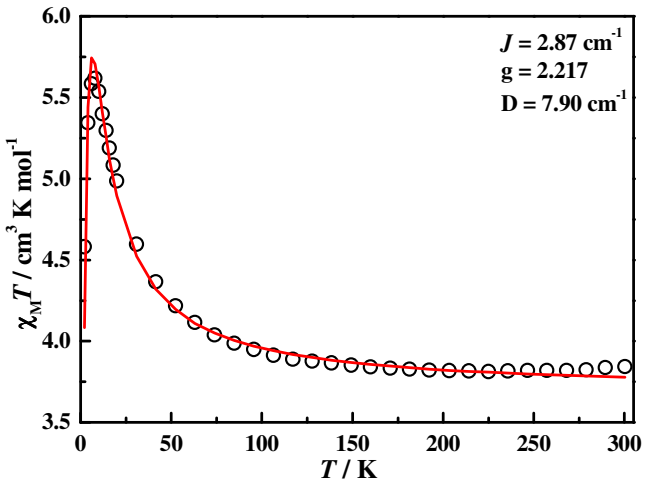

Fig. S7 Fittings of the $\chi_M T$ vs T of $[Ni^{II}_3(L^{sal-pip})_2(Propionate)_4]$ (**4**) between 2.0 and 300.0 K. The experimental data is shown as black circles and the red line corresponds to the theoretical values.

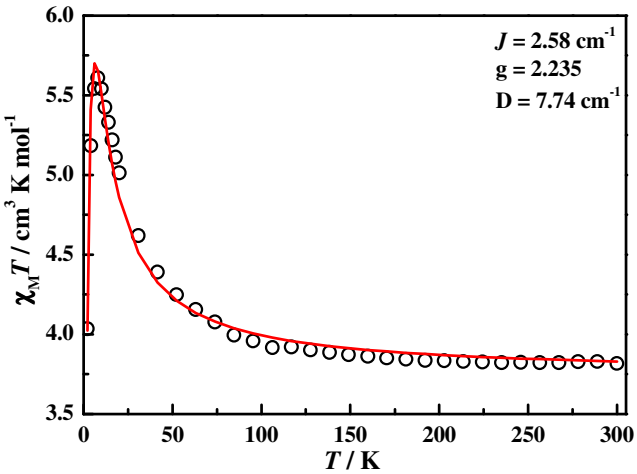

Fig. S8 Fittings of the $\chi_M T$ vs T of $[Ni^{II}_3(L^{sal-pip})_2(Benzoate)_4]\cdot CH_2Cl_2$ (**5**) between 2.0 and 300.0 K. The experimental data is shown as black circles and the red line corresponds to the theoretical values.

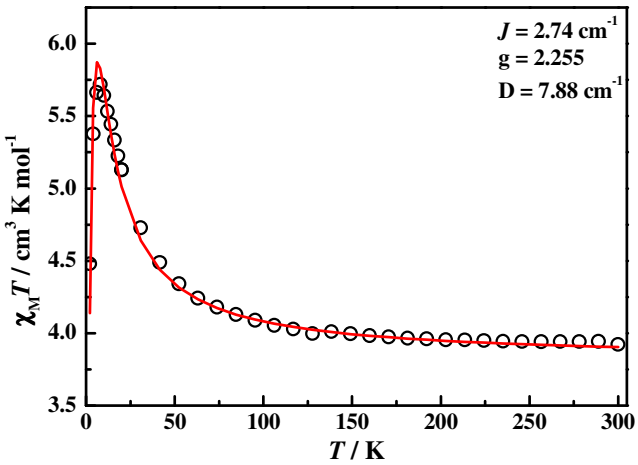

Fig. S9 Fittings of the $\chi_M T$ vs T of $[Ni^{II}_3(L^{sal-mor})_2(Propionate)_4]$ (**6**) between 2.0 and 300.0 K. The experimental data is shown as black circles and the red line corresponds to the theoretical values.

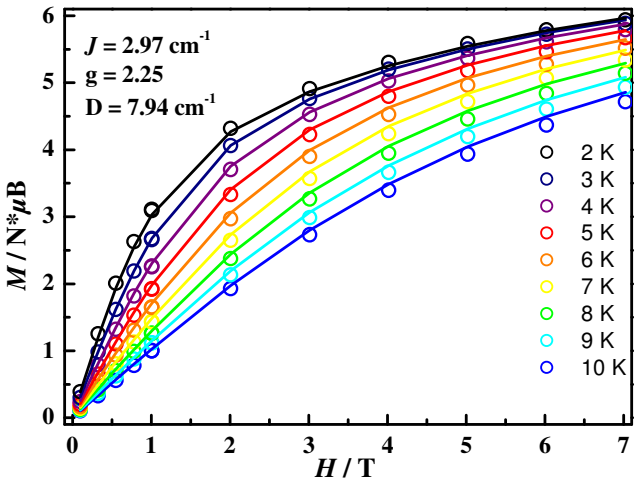

Fig. S10 The low-temperature magnetization of $[Ni^{II}_3(L^{sal-pyr})_2(Benzoate)_4]\cdot CH_3CN$ (**2**) obtained at the indicated applied dc fields. The symbols are experimental data, while the solid lines represent the calculated curves listed in the inset.

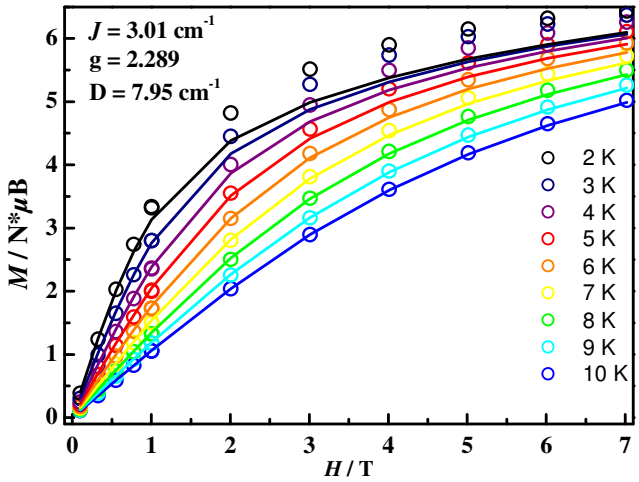

Fig. S11 The low-temperature magnetization of $[Ni^{II}_3(L^{sal-pip})_2(Acetate)_4]\cdot 2CH_3CN$ (**3**) obtained at the indicated applied dc fields. The symbols are experimental data, while the solid lines represent the calculated curves listed in the inset.

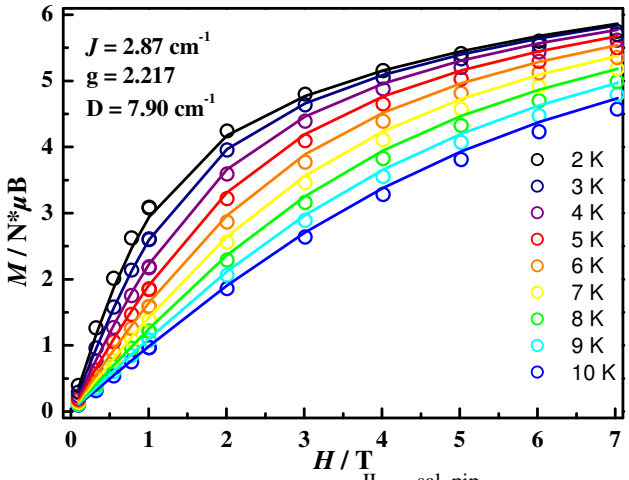

Fig. S12 The low-temperature magnetization of $[Ni^{II}_3(L^{sal-pip})_2(Propionate)_4]$ (**4**) obtained at the indicated applied dc fields. The symbols are experimental data, while the solid lines represent the calculated curves listed in the inset.

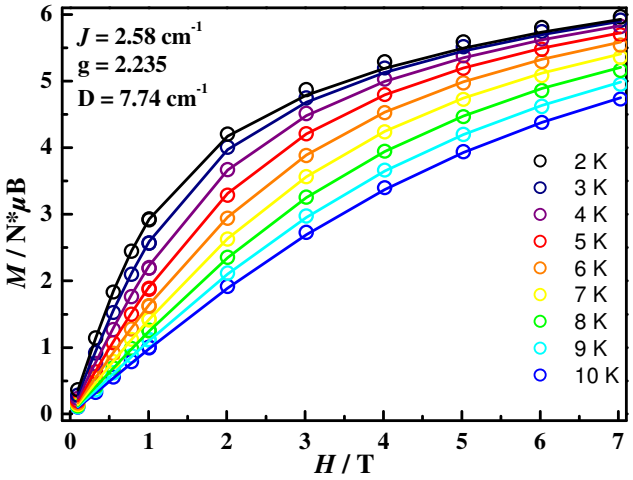

Fig. S13 The low-temperature magnetization of $[Ni^{II}_3(L^{sal-pip})_2(Benzoate)_4]\cdot CH_2Cl_2$ (**5**) obtained at the indicated applied dc fields. The symbols are experimental data, while the solid lines represent the calculated curves listed in the inset.

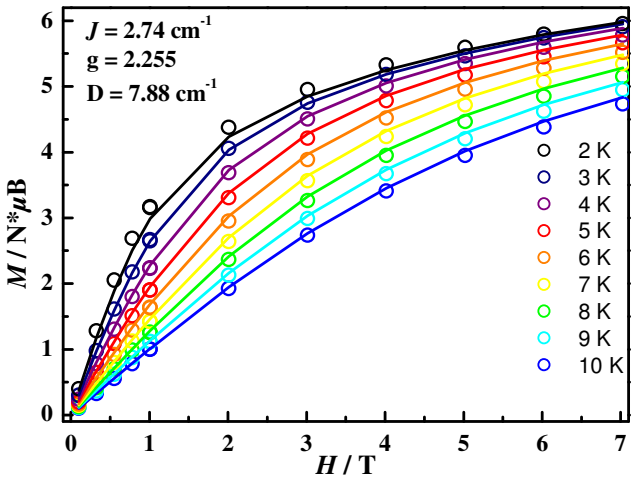

Fig. S14 The low-temperature magnetization of $[Ni^{II}_3(L^{sal-mor})_2(Propionate)_4]$ (**6**) obtained at the indicated applied dc fields. The symbols are experimental data, while the solid lines represent the calculated curves listed in the inset.

.